

On the Fundamental Concepts underlying Henry-law Adsorption and Adsorbed Gas Transport in Porous Solids

John H. Petropoulos*

Physical Chemistry Laboratory, Democritus Nuclear Research Center, Aghia Paraskevi, Athens, Greece

Vassiliki I. Havredaki

Physical Chemistry Laboratory, University of Athens, Navarinou Street, Athens, Greece

The basic concepts of the theories of adsorption and adsorbable gas flow (with particular emphasis on the latter) are examined critically in the light of (i) model calculations supplementing previous results of Nicholson and Petropoulos and (ii) new data on the permeability of a series of gases through a mesoporous colloidal graphite compact. The results of (i) indicate that the usual concepts of a constant surface diffusion coefficient and corresponding activation energy (E_s) are tenable, at least approximately, for sufficiently strong adsorption and narrow pores; but, even in this case, the parameters in question lack the physical meaning conventionally attributed to them. These results lead to notable new physical insights, particularly in connection with the relation between the values of E_s and of the energy of adsorption observed experimentally. The data of (ii) confirm the breakdown of the conventional surface flow theory in the weaker adsorption region, in accord with the predictions of the *ab initio* calculation approach of Nicholson and Petropoulos. The effect of pore size predicted by the said approach also helps to explain the difference between the flow behaviour reported here and that observed previously on similar graphite compacts of smaller pore size.

The theories of gas adsorption and flow in porous adsorbents are based on the concept of the Gibbs excess concentration and a comparable concept of 'excess flow' (referred to as 'surface flow', or more recently as 'extra flow'), respectively.^{1,2} By means of *ab initio* calculations of gas flow in model pores (or model porous media) in the Henry law adsorption and Knudsen diffusion regimes, Nicholson and Petropoulos³⁻⁶ examined critically the theory based on the latter concept with the following results.

In the stronger adsorption region (higher gas adsorbability, low temperature) the fundamental functional dependence of the 'excess flow' on the adsorption field strength and the temperature, predicted by the above conventional surface flow theory (in spite of its shortcomings), is confirmed. The significance of other important concepts of this theory, namely that of the surface diffusion coefficient and the activation energy of surface diffusion, can similarly be examined by complementing the flow results of Nicholson and Petropoulos with the corresponding adsorption calculations. This task is undertaken here.

In the low-adsorption region (low gas adsorbability, high temperature) negative excess flows were found. Hence, conventional surface flow theory breaks down completely (since the relevant surface diffusion coefficient is negative). An inversion of the normal tendency of the 'reduced permeability' $P\sqrt{M/T}$ (where P is the gas permeability, M the molecular weight of the gas and T the temperature) to decrease with diminishing gas

adsorbability or increasing temperature was also predicted. These theoretical results yielded a natural explanation of earlier (originally misinterpreted) observations⁷ of such inversion phenomena in 'Vycor' porous glass at elevated temperatures (which have lately been confirmed⁸). Similar phenomena have been observed by us⁹ at ambient temperatures in silica and alumina porous diaphragms.

These experimental observations notwithstanding, inversion phenomena of the type described above are still a rarity and had not been detected in our previous extensive measurements of the flow of weakly adsorbed gases in microporous colloidal graphite compacts.¹⁰ The results of Nicholson and Petropoulos⁴⁻⁶ suggest, however, that for sufficiently narrow or constricted pores, even the adsorbability of helium may be too high for an inversion phenomenon to appear at ambient temperatures. If so, the effect in question may be expected at larger effective pore sizes. In the present paper, we report gas permeability data for a mesoporous colloidal graphite compact, which strikingly confirm this expectation.

Adsorption and Diffusion in the Stronger Adsorption Region

The theoretical description of adsorption and flow referred to in the previous section is given by:^{1, 2, 10}

$$C = \varepsilon C_g + AC_s = (\varepsilon + Ak_s) C_g \quad (1)$$

and

$$P = P_g + P_s = \varepsilon D_g + Ak_s D_s \quad (2)$$

respectively, where C is the concentration (per unit volume of the porous medium) of adsorbed gas in equilibrium with a gas-phase concentration C_g ; C_s is the corresponding excess Gibbs concentration or concentration of adsorbed gas (per unit surface area) and k_s is the Henry adsorption constant; ε is the porosity and A the specific surface area (per unit volume of porous medium) accessible to gas; P_g is the (expected) permeability of the same gas in the absence of adsorption ('calibration gas') and P_s is the observed 'excess permeability' (conventionally attributed to flow of the adsorbed gas molecules); D_g, D_s are the corresponding gas-phase and surface diffusion coefficients. D_g can be evaluated for model pores of simple geometrical shape on the basis of a suitable assumption concerning the nature of the scattering of the gas molecules at the pore walls. Normally, scattering is assumed to be perfectly diffuse and this postulate is maintained in the work of Nicholson and Petropoulos.³⁻⁶ On this basis, we have:^{1, 3}

$$D_g = \kappa_g k_1 r_h \bar{v}_1 = \kappa_g k_1 \frac{\varepsilon}{A} \sqrt{\left(\frac{RT}{2\pi M}\right)} \quad (3)$$

where R is the gas constant; r_h is the hydraulic radius of the model pore set equal to that of the porous medium (ε/A); \bar{v}_1 is the one-dimensional mean gas molecular speed; k_1 is a geometrical factor depending on the cross-sectional shape and length to radius ratio of the model pore ($k_1 = 16/3$ for a long cylinder); and κ_g is another geometrical or structure factor incorporating all deviations of real pore structure from that of the model pore.

Conventional Surface Flow Approach

To evaluate D_s , the adsorbed gas is conventionally regarded as a dilute monolayer on the pore wall surfaces and surface flow as a two-dimensional random walk of mean step length λ_s . Because of its atomic structure, the pore wall surface (even when free of defects) is energetically heterogeneous. The admolecules are preferentially located at 'adsorption sites' (molar adsorption interaction energy E^*), wherein they are laterally confined by potential barriers of height E^\ddagger (per mol).

Only admolecules possessing activation energy $E_s = E^\ddagger$ (*i.e.* adsorption interaction energy $E^* - E^\ddagger$) contribute to surface flow. Hence eqn (2) may be conveniently rewritten as:

$$\phi = \frac{P}{P_g} = 1 + \frac{P_s}{P_g} = 1 + \phi_s = 1 + \frac{Ak_s D_s}{\epsilon D_g} = 1 + \frac{Ak_s^\ddagger D_s^\ddagger}{\epsilon D_g} \quad (4)$$

where ϕ differs from $P\sqrt{(M/T)}$ only by a constant and k_s^\ddagger and D_s^\ddagger refer to activated admolecules.³ A model energetically heterogeneous surface comprising one type of adsorption site ($E^* = E_0^* = \text{constant}$) and one type of activated admolecule site ($E^\ddagger = E_0^\ddagger = \text{constant}$) is considered (E_0^* and E_0^\ddagger may be regarded as representative averages of the variable E^* and E^\ddagger of imperfect real surfaces).

In eqn (4), D_s^\ddagger is evaluated from^{3, 11}

$$D_s^\ddagger = \kappa_s k_2 \lambda_s \bar{v}_1 = \kappa_s k_2 a_s \bar{v}_1 \quad (5)$$

where a_s is the distance between neighbouring adsorption sites, k_2 is a geometrical factor dependent on the nature of the surface atom lattice¹¹ and κ_s is a structure factor analogous to κ_g (except for the fact that it is also affected by gas adsorbability and temperature¹²).

The evaluation of k_s and k_s^\ddagger is based on suitable approximations to the adsorption potential function, which may be represented as $U = U_0(x, y)F(z)$, where x, y and z denote the spatial coordinates parallel and normal to the surface, respectively.¹³ $F(z)$ describes the shape of the adsorption potential well, which may be represented as a 9:3 potential,^{3, 14} *i.e.* (assuming an isolated surface, *cf.* line D of fig. 1):

$$F(z) = 2.598 \left[\left(\frac{z_0}{z} \right)^9 - \left(\frac{z_0}{z} \right)^3 \right] \quad (6)$$

where z_0 represents the distance of closest approach of a gas molecule to the surface layer of atoms of the solid. $U_0(x, y)$ is the depth of the adsorption potential energy well (in J mol^{-1}), which varies periodically along the surface between E_0^* and $E_0^* - E_0^\ddagger$. The precise form of the $U_0(x, y)$ function is of minor importance for the evaluation of k_s, k_s^\ddagger . Hence, we adopt here the simplified square-wave representation of Steele and Halsey,¹⁵ according to which U_0 here takes two values only, namely $U_{01} = U_{02} = E_0^*$ or $U_{01} = U_{02} = E_0^* - E_0^\ddagger$. Eqn (6) does not yield analytical expressions for k_s and k_s^\ddagger ; but for $U_0 \gg RT$ the simple harmonic oscillator approximation leads to

$$k_{s1} = \frac{\bar{v}_1}{v_{z1}} \exp \frac{U_{01}}{RT} = 0.5793 \left(\frac{RT}{U_{01}} \right)^{\frac{1}{2}} \exp \frac{U_{01}}{RT} \quad (7)$$

where $k_{s1} = k_{s1}$ (adsorption site) or $k_{s1} = k_{s2} = k_s^\ddagger$ (activated admolecule); and the second version of eqn (7) is derived by evaluating the simple harmonic oscillation frequency v_{z1} on the basis of eqn (6).¹⁶ It is usually considered that $k_s = k_{s1}$. Strictly speaking, however, one should write¹⁵

$$k_s = \gamma_s k_{s1} + (1 - \gamma_s) k_s^\ddagger \quad (8)$$

where γ_s is the fraction of A covered by adsorption sites. On the basis of $k_s \approx k_{s1}$ and eqn (4), (5) and (7), we find

$$\begin{aligned} D_s &= \frac{k_s^\ddagger D_s^\ddagger}{k_s} = \frac{\kappa_s k_2 a_s \bar{v}_1 v_{z1}}{v_{z2}} \exp \frac{U_{02} - U_{01}}{RT} \\ &= \kappa_s k_2 a_s \left(\frac{RTE_0^*}{2\pi M(E_0^* - E_0^\ddagger)} \right)^{\frac{1}{2}} \exp \left(-\frac{E_0^\ddagger}{RT} \right) \end{aligned} \quad (9)$$

$$= K_D (RT/M)^{\frac{1}{2}} \exp (-E_s/RT) \quad (9a)$$

where K_D is constant for constant E_0^\ddagger/E_0^* .

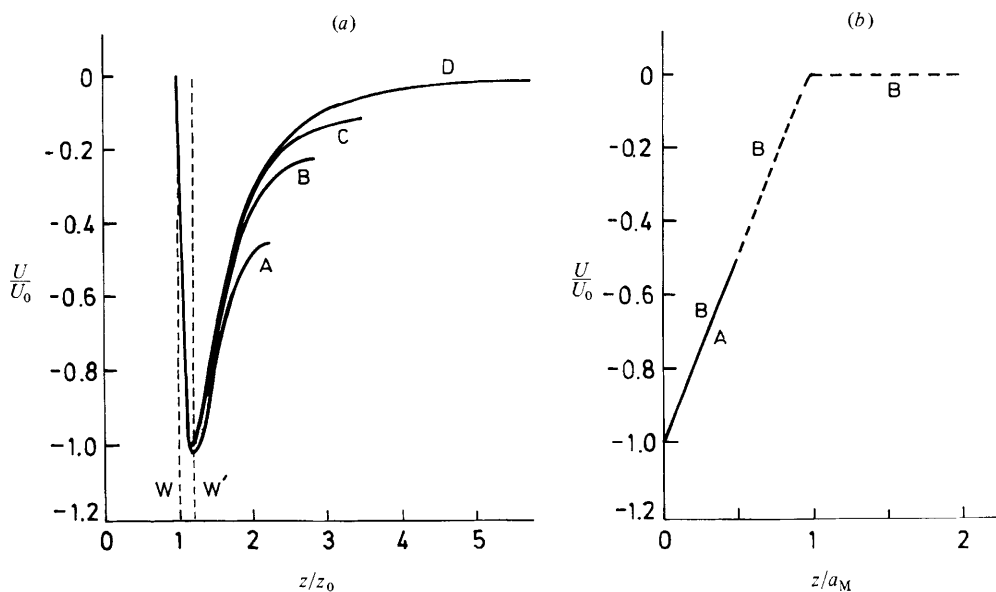


Fig. 1. (a) 9:3 adsorption potential in slit-shaped pores, $U_i(z_a \leq z \leq z_M)$, for $z_M/z_0 = 2.25$ (A), 2.85 (B), 3.50 (C), ∞ (D), with $z_a = z_0$ (W) or $z_a = z_{\min}$ (W'); (b) model triangular adsorption potential in slit-shaped pores $U_i(0 \leq z \leq z_M)$ for $z_M/a_M = \frac{1}{2}$ (A) and $z_M/a_M = 2$ (B).

Ab-initio Calculation of ϕ_s Approach

The *ab-initio* calculations of the reduced excess flow ϕ_s reported by Nicholson and Petropoulos⁴⁻⁶ refer to model pores with energetically homogeneous (structureless) wall surfaces. Hence, in terms of the treatment of the preceding subsection, all ad molecules therein must be considered as activated and the corresponding Henry law adsorption constant should be equivalent to k_s^\ddagger here. Furthermore, the calculated ϕ_s values are not significantly affected by the introduction of the lateral periodic potential $U_0(x, y)$.⁵ It is therefore evident that the aforesaid ϕ_s calculations, in conjunction with the corresponding k_s^\ddagger ones reported below, provide a method of evaluating D_s^\ddagger , which circumvents all the assumptions of conventional theory leading to eqn (5). One may similarly deduce D_s by evaluating k_s for the model heterogeneous surface defined above. It is thus possible to establish if the concept of surface diffusion coefficient is tenable, at least formally.

The requisite k_{si} may be obtained from

$$k_{si} = \int_{z_a}^{z_M} \left[\exp\left(-\frac{U_i(z)}{RT}\right) - 1 \right] dz \quad (10)$$

and k_s from eqn (8). In eqn (10), z is the distance of the gas molecule from the pore wall with $z = z_a$ or $z = z_M$ for a gas molecule in contact with the pore wall or at the centre of the pore, respectively. The effective radius of the pore is thus $r = z_M - z_a$. Nicholson and Petropoulos⁶ found that the behaviour of ϕ_s for two-dimensional slit, or cylindrical, model pores was very similar. Accordingly, here we confine attention to the former, for which more accurate and extensive data are available. $U_i(z)$ in slit-shaped pores was represented as follows:³⁻⁵

(a) 9:3 Potential [cf. fig. 1(a)]

Here eqn (6) is used with additional terms (due to the interaction of the gas molecule with both walls of the slit), namely

$$U_i(z) = 2.598 U_{0i} \left[\left(\frac{z_0}{z} \right)^9 - \left(\frac{z_0}{z} \right)^3 + \left(\frac{z_0}{2z_M - z} \right)^9 - \left(\frac{z_0}{2z_M - z} \right)^3 \right] \tag{11}$$

where U_{0i} is the depth of the adsorption potential-energy well when $z_M \rightarrow \infty$. For finite z_M the depth of the adsorption potential well U_{mi} is higher: $U(z_0 < z < z_M) = -U_{mi}$ at $z = z_{min}(U_{mi} \geq U_{0i})$. Normally, in eqn (10), $z_a = z_0$; but, in ref. (5) and (6), it was mathematically convenient to set $z_a = z_{min}$. As shown later, the choice of z_a makes no difference to the adsorption behaviour of interest here.

(b) Model Triangular Adsorption Potential [cf. fig. 1(b)]

Here,
$$U_i(z) = -U_{0i}(1 - z/a_M) \tag{12}$$

for $0 \leq z \leq a_M$, if $z_M > a_M$; or for $0 \leq z \leq z_M$, if $z_M \leq a_M$; and

$$U_i(z) = 0 \tag{12a}$$

for $a_M < z \leq z_M$; if $z_M > a_M$. In eqn (12), a_M is the maximum width (at the top) of the triangular potential well at an isolated surface; U_{0i} is the depth of the well (independent of z_M , i.e. $U_{mi} = U_{0i}$); and $z_a = 0$. Physically, this potential is artificial (it corresponds to a constant force emanating from the pore wall and vanishing abruptly at $z = a_M$, if $z_M < a_M$; or at $z = z_M$, if $z_M \leq a_M$), but it is mathematically simple [it leads to an analytical result for eqn (10)] and also provides useful insight into the effect of the functional form of $U_i(z)$.

For the type of model pores considered here $r = r_h$. Furthermore, it is convenient to define a dimensionless radius $R = r/a$ (where $a = z_0$ or $a = a_M$ in the case of the 9:3 and triangular adsorption potentials, respectively) and a dimensionless adsorption potential energy $\bar{U} = U/RT$.

Results and Discussion

Adsorption Parameters

Examples of the results of model calculations of k_{si} and k_s based on the treatment described above are given in fig. 2 and 3. The reported k_s values refer to a model energetically heterogeneous surface described by eqn (8) with $\gamma_s = \frac{1}{3}$ and $U_{02}/U_{01} = 0.60$ corresponding to $E_0^*/E_0^* = 0.40$.

Lines A, B and C in fig. 2 illustrate the effect of different choices of adsorption potential on the $\ln k_{si}$ vs. $\bar{U}_{0i}(= U_{0i}/RT)$ plot for an isolated surface. In the region $\bar{U}_{0i} \approx 2-8$, these plots can be represented to a reasonable approximation by straight, nearly parallel lines [cf. ref. (16)] given by

$$k_{si} = k_{si}^0 \exp(\alpha_s U_{0i}/RT) \tag{13}$$

where $\alpha_s \approx 0.82-0.86$. Fig. 2 and 3 further show that k_{si} for narrow pores or k_s for energetically heterogeneous pore surfaces behave similarly, except for differences in the value of α_s . As the pore radius decreases, α_s tends to increase ($\alpha_s \approx 0.87$ for line H, and $\alpha_s \approx 0.92$ for line I, in fig. 3), although this tendency is markedly reduced if k_{si} is made a function of \bar{U}_{mi} ($\alpha_s \approx 0.85$ for line I' in fig. 3). Fig. 2 shows that the plots of $\ln k_s$ vs. \bar{U}_{01} tend to be appreciably less steep ($\alpha_s \approx 0.77$ for line D; $\alpha_s \approx 0.74$ for line E) than the corresponding $\ln k_{si}$ vs. \bar{U}_{01} plots (represented by lines A, $\alpha_s \approx 0.85$, and B, $\alpha_s \approx 0.82$, respectively). One may similarly fit eqn (13) to the k_{si} values obtained from eqn (7), or the k_s values obtained from eqn (7) and (8), in the range of $\bar{U}_{0i}(\bar{U}_{01}) \approx 2-8$ (cf. fig. 2).

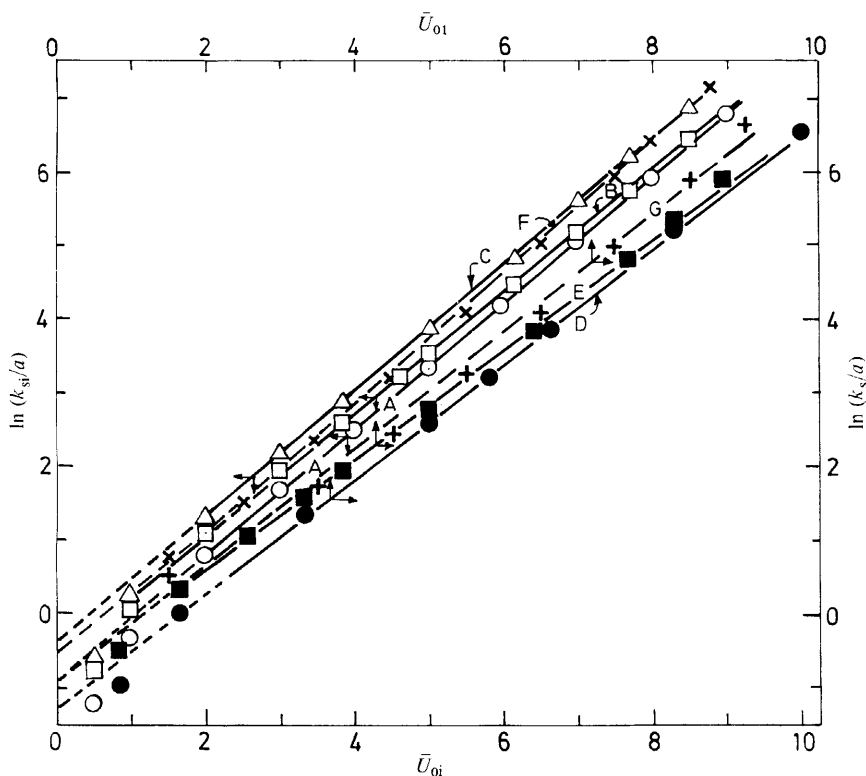


Fig. 2. Adsorption constants k_{si} (lines A, B, C and F) and related k_s of eqn (8) (lines E, D and G) for isolated flat surfaces ($z_M \rightarrow \infty$) calculated by (i) the conventional treatment of eqn (7) (lines F and G), or (ii) the present treatment of eqn (10), in conjunction with either eqn (11) [$z_a = z_0$ (C), $z_a = z_{min}$ (lines B and E)] or eqn (12) and (12a) (lines A and D).

The resulting α_s are perceptibly higher than those recorded for isolated surfaces above ($\alpha_s \approx 0.90$ for line F; $\alpha_s \approx 0.81$ for line G), but the adsorption behaviour predicted by eqn (7) and (10) is otherwise very similar at $\bar{U}_{oi} > 2$ [cf. ref. (16) and note that the significant discrepancies referred to in ref. (14) probably arise from incorrect evaluation of v_{zi}].

It is worth noting that conformity of k_s to eqn (13) is equivalent to a constant energy of adsorption $\Delta E_s = -\alpha_s U_{oi} = -\alpha_s E_0^*$, since

$$k_s = k_s^0 \exp(-\Delta E_s/RT). \quad (14)$$

The results for α_s reported above indicate that the values of $-\Delta E_s$ predicted by the treatment of eqn (10) are somewhat lower than those given by the conventional treatment, which in turn tend to be somewhat lower than E_0^* (or U_{mi} in the case of narrow pores) in the E_0^*/RT range of chief practical interest.

Surface Diffusion Parameters

The higher values of the reduced excess flow ϕ_s (namely $\phi_s \gtrsim 3$) calculated by Nicholson and Petropoulos⁶ can be represented to a reasonable approximation by analytical expressions analogous to that for k_{si} (k_s) given above:¹⁷

$$\phi_s = K_0 R^{-m} \exp(\alpha U_{02}/RT) \quad (15)$$

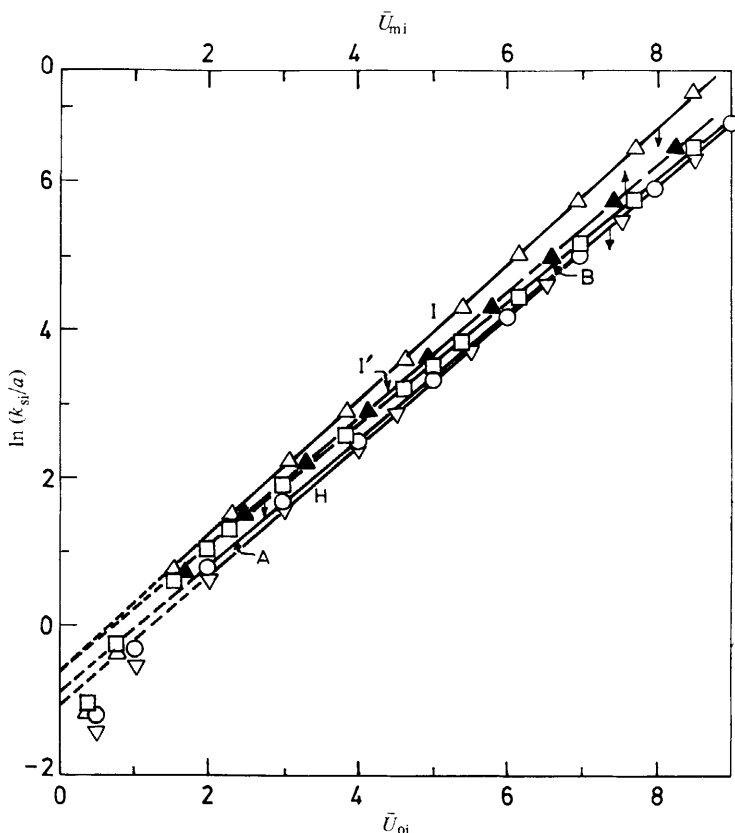


Fig. 3. Adsorption constants k_{si} for isolated surfaces (lines A and B) or narrow pores (lines H, I and I'), with 9:3 ($z_a = z_{min}$, lines B, I and I') or model triangular (lines A and H) adsorption potential, as a function of \bar{U}_{oi} (lines A, B, I and H) or \bar{U}_{mi} (line I'). (Note that $\bar{U}_{mi} = \bar{U}_{oi}$ for lines A, B and H.)

where K_0 , m and α are empirical constants. Data in the appropriate range were obtained for $R = 0.5-2.5$ (pore length to radius ratio = 20) and $R = 1.05-2.30$ (pore length to radius ratio ≈ 10) for the triangular and 9:3 ($z_a = z_{min}$) adsorption potentials, respectively, yielding $\alpha \approx 0.78-0.79$, $m \approx 2.1$, $K_0 \approx 0.045$ (triangular potential); or $\alpha \approx 0.79-0.82$, $m \approx 2.8-3.0$, $K_0 \approx 0.15$ (9:3 potential).

From eqn (3), (4), (13) and (15) an approximate analytical expression for D_s^\ddagger for the model pore ($\kappa_s = 1$) can be deduced:

$$D_s^\ddagger = \frac{k_1 \bar{v}_1 r^2 \phi_s}{k_s^\ddagger} = \frac{K_0 k_1 \bar{v}_1 a^2 R^{2-m}}{k_{s2}^0} \exp \frac{(\alpha - \alpha_s) U_{02}}{RT} \tag{16}$$

which, in the case of the triangular potential, reduces, to a first approximation ($m \approx 2$, $\alpha \approx \alpha_s$) to the form of eqn (5):

$$D_s^\ddagger \approx (K_0 k_1 a^2 / k_{s2}^0) \bar{v}_1. \tag{16a}$$

Note, however, that the constant factor in eqn (16a) is not determined by structural characteristics of the surface as implied by eqn (5). In fact, as suggested by eqn (16) (since $\alpha < \alpha_s$) and shown in fig. 4, there is a noticeable downward drift of D_s^\ddagger with

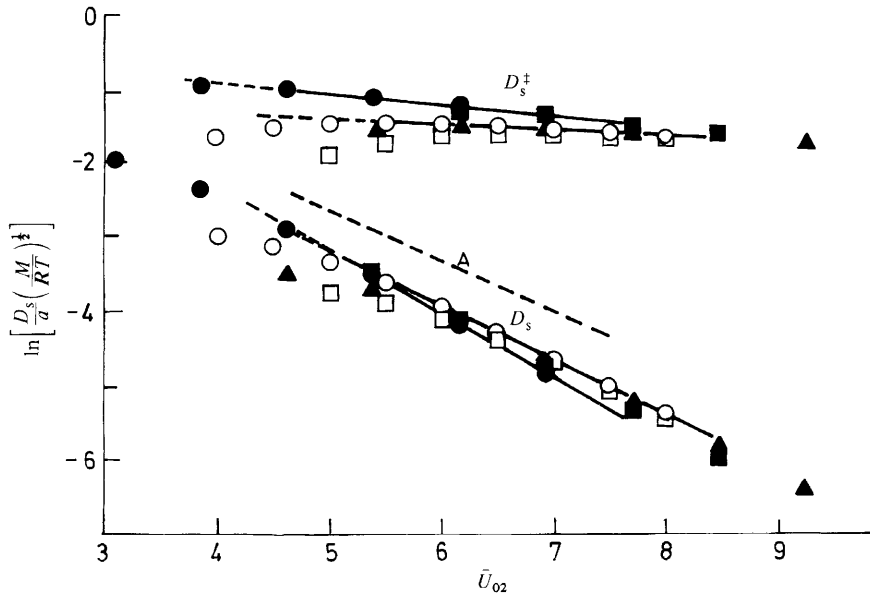


Fig. 4. Surface diffusion coefficients D_s and corresponding D_s^+ calculated from the numerical data of ref. (5) and (6) and of the present work; 9:3 adsorption potential ($z_a = z_{\min}$): $R = 1.05$ (●), 1.65 (■), 2.30 (▲); model triangular adsorption potential: $R = 1$ (○), 1.5 (□). The slope of a D_s plot corresponding to $E_s = E_0^+ (= \frac{2}{3}\bar{U}_{02})$ is indicated by line A.

increasing \bar{U}_{02} . The more marked downward trend of D_s^+ (with decreasing \bar{U}_{02}) in the lower \bar{U}_{02} region is simply due to breakdown of eqn (15) ($\phi_s < 3$), when \bar{U}_{02} and R are not sufficiently high and low, respectively. Fig. 4 further shows that the behaviour of D_s^+ in the case of the 9:3 potential is not materially different. The lack of a reasonably clear-cut analytical approximate result in this case is no doubt attributable to the significant dependence of $U_1(z)$ on R in the range $R = 1.05$ – 2.30 (corresponding to $z_M = 2.25$ – 3.50) used [cf. fig. 1(a)], in contrast to the complete lack of such dependence when $R \geq 1$, in the case of the triangular potential [cf. fig. 1(b)].

One may similarly evaluate D_s for the model pore with energetically heterogeneous pore wall surface, to obtain

$$D_s = \frac{k_1 \bar{v}_1 r^2 \phi_s}{k_s} \approx \frac{K_0 k_1 \bar{v}_1 a^2 R^{2-m}}{k_{s1}^0} \exp \frac{\alpha U_{02} - \alpha_s U_{01}}{RT}. \quad (17)$$

Comparison of eqn (17) with eqn (9) shows that the activation energy of surface diffusion E_s (which is conventionally identified with E_0^+) is here given by

$$E_s = \alpha E_0^+ + (\alpha_s - \alpha) E_0^*. \quad (18)$$

Since $\alpha_s > \alpha$ (note that α_s must be determined in the \bar{U}_{01} range corresponding to the \bar{U}_{02} region used in the determination of α , hence the α_s values applicable here are significantly higher than those previously deduced from fig. 2 and 3), E_s can exceed E_0^+ appreciably, as indicated by the slopes of the D_s plots of fig. 4.

In practice, the chief quantity of interest is the ratio $-E_s/\Delta E_s$ which, according to the conventional treatment of eqn (7) and (9), should not differ materially from E_0^+/E_0^* . However, the experimental values of $-E_s/\Delta E_s$ typically quoted^{1,2,10} are of the order of 0.6 or higher, whereas values of E_0^+/E_0^* obtained by model calculations are markedly lower (e.g. $\lesssim 0.3$).^{16,18} As shown above, the present treatment predicts higher E_s and

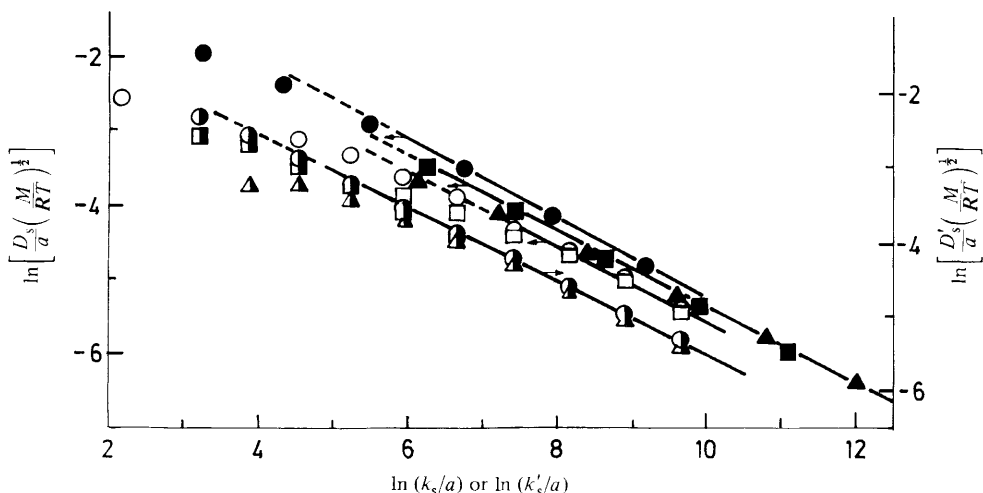


Fig. 5. Surface diffusion coefficients in relation to the corresponding k_s ; D_s , k_s (\circ , \square , \bullet , \blacksquare , \blacktriangle) were calculated exactly as for fig. 4; for D'_s , k'_s (\odot , \blacksquare , \blacktriangle) a calibration gas of finite adsorbability ($\bar{U}_{02} = 0.5$) was assumed; 9:3 adsorption potential: $R = 1.05$ (\bullet), 1.65 (\blacksquare), 2.30 (\blacktriangle); model triangular adsorption potential: $R = 1$ (\circ , \odot), $R = 1.5$ (\square , \blacksquare), $R = 2.5$ (\triangle); $-E_s/\Delta E_s$ (deduced from the linear parts of the plots) ≈ 0.49 (\circ , \square), 0.52 (\bullet), 0.50 (\bullet , \blacktriangle), 0.49 (\odot , \blacksquare , \blacktriangle). Note that the D'_s plots have been displaced downwards for clarity.

lower $-\Delta E_s$ (especially when energetic surface heterogeneity is taken into account) than the conventional one and thus helps partly to explain this discrepancy. The actual predicted values of $-E_s/\Delta E_s$ for the model pores and the model energetically heterogeneous surface assumed here can be determined directly from the slope of plots of the calculated $\ln [(D_s/a)(M/RT)^{1/2}]$ vs. $\ln (k_s/a)$, since eqn (14), (17) and (18) yield

$$\ln [(D_s/a)(M/RT)^{1/2}] = \ln K'_D - \frac{E_s}{\Delta E_s} \ln k_s^0 + \frac{E_s}{\Delta E_s} \ln k_s \tag{19}$$

where K'_D is a constant. The relevant plots (fig. 5) show good linearity in the high k_s region with slopes which are remarkably insensitive to the value of R or the form of the adsorption potential [the only perceptible difference is found in the case of the narrowest pore with 9:3 potential where, as shown by line (A) of fig. 1(a), the adsorption force fields emanating from opposite pore walls overlap extensively]. The resulting values of $-E_s/\Delta E_s$ exceed the value of E_0^*/E_0^* assumed here by ca. 20%. Fig. 5 also includes examples from a further series of calculations intended to simulate the fact that, in practice, ϕ_s is of necessity determined in relation to a calibration gas of finite adsorbability (usually He). Values of E_0^* as high as 2.5 kJ mol⁻¹ have been quoted for He.¹⁵ Accordingly, surface diffusion coefficients D'_s were calculated assuming a calibration gas with $\bar{U}_{02} = (E_0^* - E_0^{\ddagger})/RT = 0.5$ (corresponding to $E_0^* = 2$ kJ mol⁻¹ at $T \approx 300$ K or $E_0^* = 2.5$ kJ mol⁻¹ at $T \approx 375$ K). The resulting plots (fig. 5) attain linearity at substantially lower k_s values, but the slope of the linear region is essentially unchanged.

A further factor which may affect the experimental value of $-E_s/\Delta E_s$ is κ_s , which should appear in eqn (16) or (17) when applied to porous media. As pointed out previously, κ_s is not independent of \bar{U}_{01} . Its effect can be studied by means of suitable model calculations, such as those of Nicholson and Petropoulos,⁶ who constructed a series of simple model porous media consisting of parallel (P) or serial (S) arrays of model pores of two different radii (R_1, R_2) combined in various proportions (number fractions f_1, f_2). Calculations of ϕ_s then showed that its dependence on \bar{U}_{02} (in the appropriate

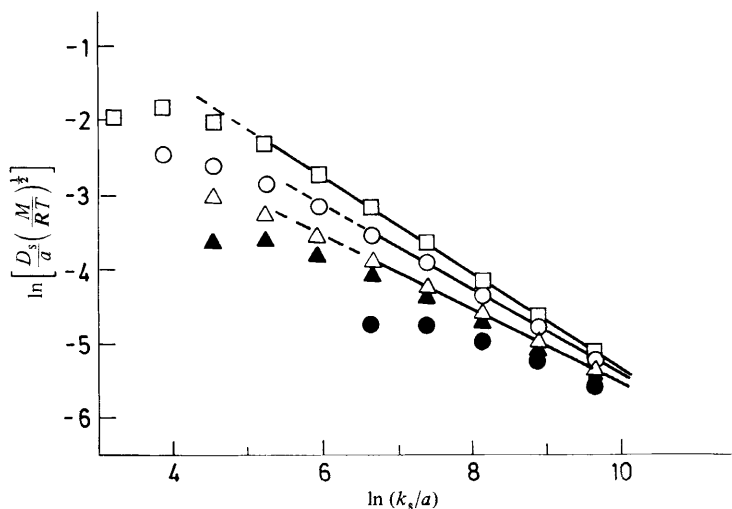


Fig. 6. Surface diffusion coefficients in relation to the corresponding k_s for model porous media consisting of parallel (▲, ●) or serial (△, ○, □) arrays of narrow ($R_1 = 1$) and wide ($R_2 = 5$) model pores with triangular adsorption potential.⁶ Number fraction of narrow pores, $f_1 = 0.9$ (△, ▲), 0.5 (○, ●), 0.1 (□). The linear parts of the serial array pore plots yield $-E_s/\Delta E_s \approx 0.49$ (▲), 0.56 (●), 0.64 (■).

range) could still be described by eqn (15); the value of α was unaffected by P-type structure, but could be considerably lower, in the \bar{U}_{02} range of practical interest, in the case of S-type (constricted pore) structure. Where k_s is concerned, the arrangement of the pores is obviously immaterial and the value of α_s will not be perturbed significantly, unless very narrow pores are present. Hence, in accordance with eqn (18), S-type pore structure should tend to enhance the value of $-E_s/\Delta E_s$. This is confirmed by the relevant plots, shown in fig. 6, which exhibit good linearity in the higher \bar{U}_{02} range. Fig. 6 further shows that the linear region of the plot becomes both more extensive and steeper, as the proportion (f_1) of narrow sections (*i.e.* constrictions) in the serial pore array becomes lower; for $f_1 = 0.1$, the value of $-E_s/\Delta E_s$ exceeds that characteristic of single pores (fig. 5) by over 25%. It is also important to note that axially non-uniform porosity (expected to be present in the vast majority of porous diaphragms studied in practice as a result of the pelletization process)¹⁹ has been shown²⁰ to have the same effect as S-type pore structure.

We conclude that the discrepancy between experimental $-E_s/\Delta E_s$ values and E_0^\ddagger/E_0^* determined by model calculations can be attributed in part to oversimplifications in the conventional surface flow approach and in part to the effect of the pore structure and macroscopic non-homogeneity of real porous media.

Another question of considerable practical importance concerns the value of $E_s/\Delta E_s$ for a series of gases in a given porous solid. If $E_0^\ddagger/E_0^* \approx$ constant within the series, the results presented in fig. 5 and 6 indicate that $E_s/\Delta E_s \approx$ constant only if the relevant k_s range falls wholly within the linear part of the $\log [D_s/(M/RT)^{1/2}]$ vs. $\log k_s$ plot pertaining to the effective mean pore size and pore structure of the porous medium concerned. If the lower end of the k_s range in question extends into the curved part of the said plot, a tendency for $-E_s/\Delta E_s$ to decrease in the case of the lighter gases is to be expected.

Detailed numerical data for k_s and D_s (using He as calibration gas) suitable for applying the above ideas are given in tables II.4 and II.5 of ref. (2). The resulting plots are shown in fig. 7. The heavier gas data for 'Carbolac' diaphragms (including such diverse gases as Ar, CH₄ and CO) are clustered remarkably closely around a straight

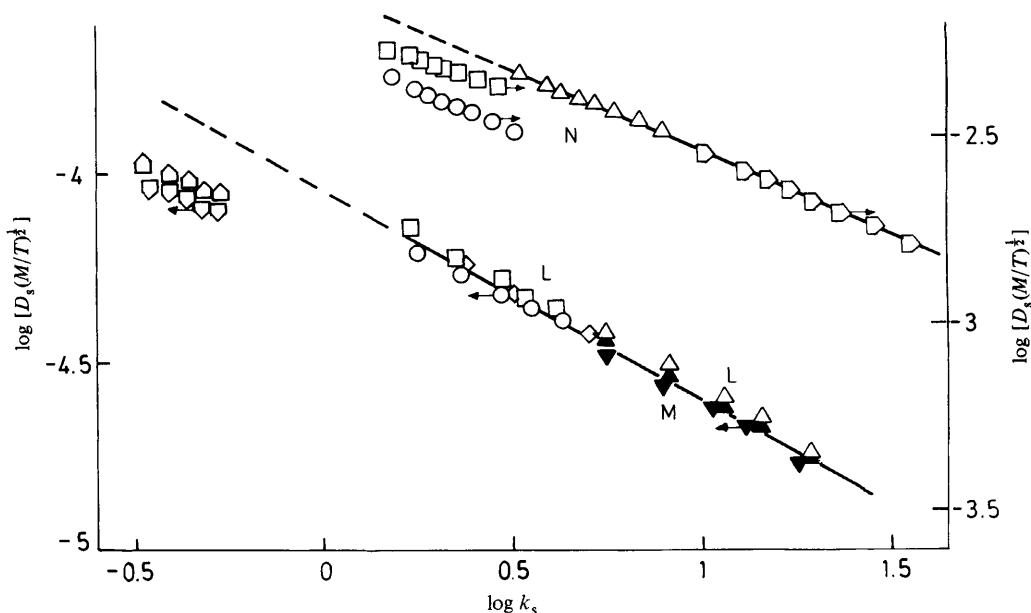


Fig. 7. Correlation based on eqn (19) between D_s (in $\text{cm}^2 \text{s}^{-1}$) and k_s (in nm) measured by Ash *et al.*² for a variety of gases, temperatures and porous diaphragms. Membrane L ('Carbolac' carbon): lower open points; Membrane M ('Carbolac' carbon): filled points; Membrane N ('Graphon' graphitized carbon): upper open points; H_2 : ∇ ; D_2 : \triangle ; N_2 : \circ ; Ar: \square ; Kr: \triangle ; Xe: \diamond ; CH_4 : ∇ ; CO: \diamond .

line corresponding to $-E_s/\Delta E_s \approx 0.56$. The points for the lightest gases (H_2 and D_2) fall well below this line and yield $-E_s/\Delta E_s \approx 0.34$ and 0.40 , respectively. The difference between the aforementioned $E_s/\Delta E_s$ values and those quoted in ref. (2) is no doubt largely due to our definition of E_s according to the Eyring transition-state theory and our method of direct evaluation of $E_s/\Delta E_s$, as opposed to the Arrhenius definition of E_s and the individual evaluation of E_s , ΔE_s used in ref. (2). In the case of the 'Graphon' diaphragm, data for four gases only are available, but the general pattern of behaviour, at least as far as defined by the noble gases, does not appear to be different. The straight line defined by the points in the high k_s region corresponds to $-E_s/\Delta E_s \approx 0.46$ as compared to $-E_s/\Delta E_s \approx 0.35$ for Ar. Hence, in this case, the diminution in $-E_s/\Delta E_s$ is noticeable at k_s values higher than before, in keeping with the larger pore size of the 'Graphon' ($r_h \approx 5$ nm) as compared with the 'Carbolac' ($r_h \approx 0.5$ nm) diaphragm.

Thus, the experimental behaviour revealed by fig. 7 is in at least qualitative accord with the theoretical results of fig. 5 and 6. On the basis of the conventional treatment, on the other hand, any variation in $-E_s/\Delta E_s$ must be interpreted in terms of a corresponding variation in E_0^\ddagger/E_0^* . Model calculations on smooth surfaces, however, show that E_0^\ddagger/E_0^* should tend to decrease for the bulkier gas molecules,¹⁶ which is the reverse of what is observed here.

Before closing this section some comment is called for in connection with the considerable shift of the N_2 points in fig. 7 for the 'Graphon' diaphragm relative to those of Ar. This is presumably attributable to the effect of specific gas-solid interactions (quadrupole interactions in the case of N_2). It is noteworthy that analogous effects are not visible in the case of the 'Carbolac' data. Clearly, this interesting point can be pursued further only in the light of more data and of suitable elaboration of the treatment of Nicholson and Petropoulos.⁵

Adsorption and Diffusion in the Weak Adsorption Region

In the weak adsorption region, the usefulness of the 'excess parameters' k_s and D_s becomes increasingly questionable from the point of view of physical meaningfulness (although the problem of reliable experimental determination is also not unimportant). The deviations of the plots of fig. 2, 3 and 4 from linearity at low \bar{U}_{01} or \bar{U}_{02} , respectively, cause ΔE_s and E_s to lose their usual physical meaning. The occurrence of negative excess flow at still lower \bar{U}_{02} , which renders D_s meaningless, has already been noted in the introductory section. The occurrence of negative Gibbs excess concentrations is also noteworthy.²¹

Accordingly, we adopt here a formulation of adsorption and flow akin to that of Nicholson and Petropoulos,^{5,6} who reported their calculated flow results in the form of $\ln \phi$ vs. \bar{U}_{02} plots. As previously pointed out, the former parameter differs only by a constant factor from the experimental 'reduced permeability' $P\sqrt{(M/T)}$. \bar{U}_{02} is less convenient from this point of view. Accordingly, it is replaced here by the logarithm of a 'reduced sorption coefficient' k which, using eqn (1), is given by

$$k = C/\varepsilon C_g = 1 + Ak_s/\varepsilon = 1 + k_s/r_h$$

and is, therefore, easily deduced here from the k_s values previously calculated. At the same time, k differs from the sorption coefficient determined experimentally, $S = C/C_g$, only by a constant factor, namely ε ; if ε is determined by helium pycnometry, then $\kappa = S/S_{\text{He}}$. One may similarly normalise $P\sqrt{(M/T)}$ with respect to He to obtain ϕ/ϕ_{He} . The advantage of this formulation is that the finite adsorbability of the 'normalizing gas' merely shifts the relevant plot parallel to the axes without changing its form. The computation results of Nicholson and Petropoulos for slit-shaped pores (together with an example for a model porous medium)^{5,6} have been plotted in this manner in fig. 8 for the cases of $E_0^\ddagger/E_0^* = 0$ or 0.4.

Experimental

A mesoporous diaphragm of cross-sectional area 0.795 cm², thickness 3.37₅ cm and porosity 0.362 was constructed by compaction of very fine graphite powder (Acheson DAG 621 dispersion powder of specific surface area 72 m² g⁻¹ and ash content 0.29%) in a cylindrical metal holder. To minimize non-uniformity of packing density, the powder was added to the holder in 15 small portions and compressed each time symmetrically by means of close-fitting pistons.⁹ The effective hydraulic radius was $r_h = \varepsilon/A = 3.6$ nm.

The gases used were of > 99.9% purity. Permeation measurements were carried out by attaching the specially designed diaphragm holder directly through soft metal gaskets to a permeation apparatus incorporating a mercury manometer and manostatic device on the upstream side and a McLeod gauge on the downstream side.⁹ The diaphragm was first thoroughly outgassed at temperatures up to 470 K. After completion of the permeation runs, the diaphragm holder was quickly transferred to a sorption bulb, which was attached to a volumetric sorption apparatus. Special metal attachments were used to minimize the dead volume of the sorption bulb. Prior to the adsorption measurements, the diaphragm was subjected to a second, thorough, but considerably milder, outgassing treatment.

Results and Discussion

Adsorption and permeation measurements were carried out for He, H₂, N₂, Ar, Kr, CH₄, C₂H₆, and CO₂ in the pressure range 30–120 Torr.† Henry's law was obeyed throughout this range for all gases, except the last two at the high-pressure end. The

† 1 Torr = 101325/760 Pa.

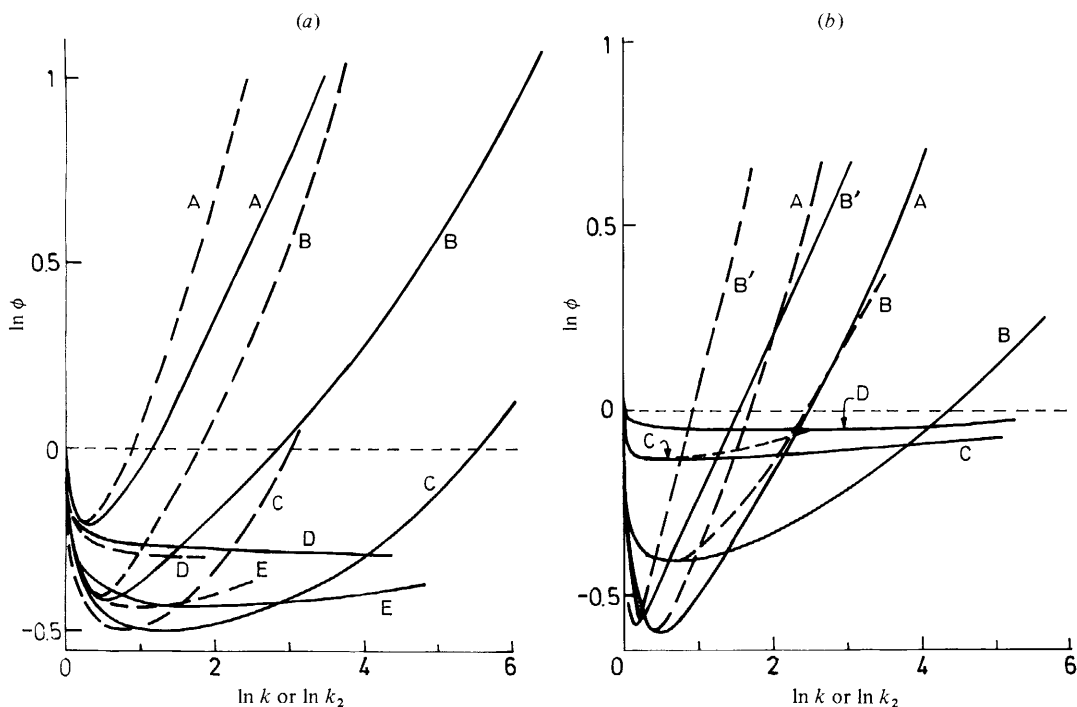


Fig. 8. Reduced permeabilities ϕ calculated for single model pores (or a model porous medium)^{5, 6} in relation to the corresponding reduced sorption coefficient k (assuming $E_0^*/E_0^* = 0.4$; full lines) or k_2 ($E_0^*/E_0^* = 0$; broken lines): (a) slits with 9:3 potential ($z_a = z_{\min}$) and $R = 1.05$ (A), 2.30 (B), 4.80 (C), 9.80 (D), 24.80 (E); (b) slits with model triangular potential and $R = 1$ (A), 3 (B), 10 (C), 25 (D); or a serial array (with $R_1 = 1$, $R_2 = 5$ and $f_1 = 0.5$) of effective dimensionless hydraulic radius $R = 3$ (B').

corresponding permeabilities were constant (and showed no definite tendency to vary, even outside the Henry law region in the case of C_2H_6 and CO_2).

The results are plotted in fig. 9(b) in the form proposed in the previous section but one, in comparison with those of Savvakis *et al.*¹⁰ on a series of compacts constructed from the same graphite powder, but of considerably smaller pore size [fig. 9(a)]. The present data exhibit an unmistakable minimum in ϕ as gas adsorbability is varied, in conformity with the general pattern predicted by the Nicholson-Petropoulos approach (fig. 8). The lack of a similar pattern in the results of ref. (10) [fig. 9(a)] can now be explained on the basis of the effect of pore size. As shown in fig. 8, the minimum in ϕ shifts to lower k as R is reduced, with the result that it will be unobservable in practice if it occurs at $k < k_{He}$ at the temperature of observation. Pore constrictions have a similar effect [*cf.* lines B and B' in fig. 8(b)]. The quantitative differences among the different diaphragms in fig. 9(a) are no doubt attributable to their diverse macroscopic structures;¹⁰ whereas the deviation of the data of fig. 9(b) from a single smooth curve are presumably largely due to specific gas-solid interactions of the kind noted earlier in the 'Graphon' diaphragm of fig. 7.

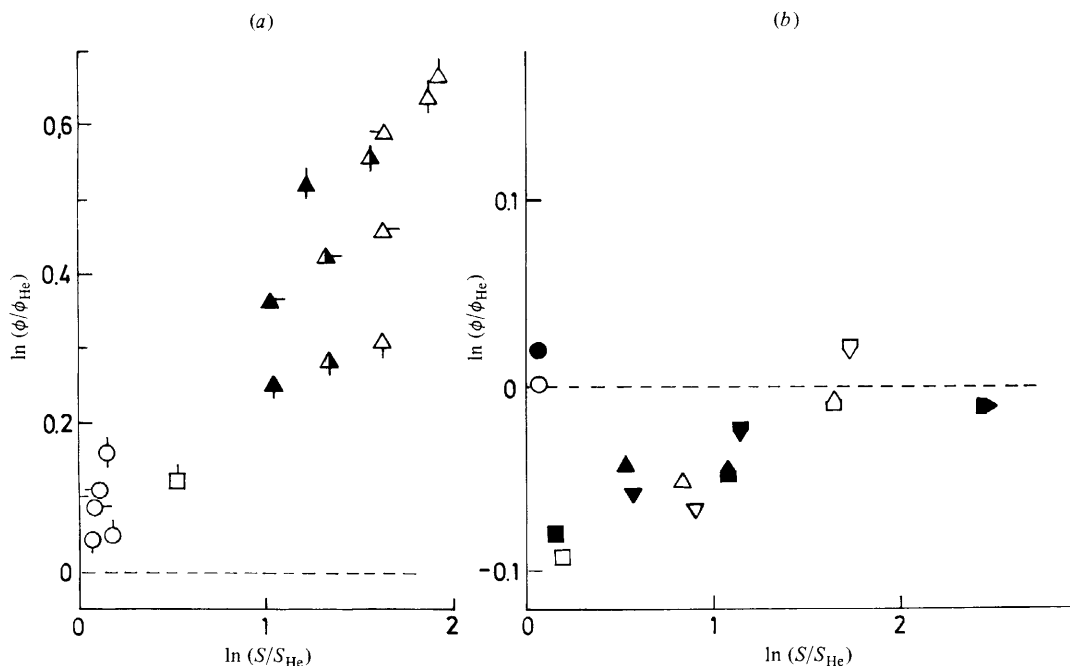


Fig. 9. Experimental reduced permeabilities in relation to the corresponding reduced sorption coefficients (normalized with respect to He in both cases) for a series of gases in a series of porous colloidal graphite compacts: (a) microporous compacts ($\epsilon/A \approx 1$ nm) C(\circ), D(\circ), E(\circ), F(\circ), G(\circ) of ref. (10) at $T = 296.4$ K (\triangle), 323 K (\blacktriangle), 348 K (\blacktriangle); (b) mesoporous compact ($\epsilon/A \approx 3.5$ nm) of present work at $T = 298.2$ K (open points), 348.2 K (filled points). Gases used: Ne(\circ), H_2 (\square), Ar (\triangle), N_2 (∇), CH_4 (\triangle), Kr (\square), CO_2 (\triangleright), C_2H_6 (\triangleleft).

Conclusion

The theoretical results obtained here indicate that, on the basis of the Nicholson–Petropoulos approach, the basic concepts of conventional surface flow theory are formally valid to a first approximation in the stronger adsorption region when applied to sufficiently narrow pores. Thus, ‘excess flow’ is indeed governed by a ‘surface diffusion coefficient’ D_s , approximately independent of pore size, and an activation energy of surface diffusion E_s ; although the value of D_s does not reflect solely the structural characteristics of the pore wall surface and E_s is not identical with the height of the lateral potential barrier E_0^\ddagger , as implied by conventional theory. The effect of pore structure on the value of E_s has also been shown to be important, with the result that the total deviations $E_s < E_0^\ddagger$ and $-\Delta E_s < E_0^*$ revealed by our model calculations go a long way towards explaining the discrepancies commonly found between $-E_s/\Delta E_s$ as determined experimentally and E_0^\ddagger/E_0^* as calculated for realistic smooth model surfaces. The correlation between $D_s\sqrt{(M/T)}$ and k_s proposed here in terms of eqn (19) has the virtue of yielding $E_s/\Delta E_s$ directly and represents a considerable advance over the empirical correlation between $P\sqrt{(M/T)}$ and k_s given by Ash *et al.*² By plotting the data of the latter authors according to eqn (19), a clear tendency for $-E_s/\Delta E_s$ to diminish at low k_s has been revealed, in accord with the Nicholson–Petropoulos treatment, but not with the conventional one.

The experimental results reported in the present paper, on the other hand, provide further strong support for the Nicholson–Petropoulos approach, particularly with regard

to the predictions of this approach concerning the dependence of flow behaviour in the weak adsorption region on pore size.

The present work was carried out at the Democritus Centre and is based in part on a Ph.D. Thesis presented by Ms V. I. Havredaki to the University of Athens. Thanks are due to Prof. Th. Yannakopoulos, Prof. R. M. Barrer and Dr D. Nicholson for useful discussions.

References

- 1 e.g. R. M. Barrer, *Appl. Mater. Res.*, 1963, **2**, 129.
- 2 R. Ash, R. M. Barrer, J. H. Clint, R. J. Dolphin and C. L. Murray, *Philos. Trans. R. Soc. London*, 1973, **275**, 255.
- 3 D. Nicholson and J. H. Petropoulos, *J. Colloid Interface Sci.*, 1973, **45**, 459.
- 4 D. Nicholson and J. H. Petropoulos, *J. Colloid Interface Sci.*, 1979, **71**, 570.
- 5 D. Nicholson and J. H. Petropoulos, *J. Colloid Interface Sci.*, 1981, **83**, 420.
- 6 D. Nicholson and J. H. Petropoulos, *J. Colloid Interface Sci.*, 1985, **106**, 538.
- 7 S. T. Hwang and K. Kammermeyer, *Can J. Chem. Eng.*, 1966, **44**, 82.
- 8 Y. Shindo, T. Hakuta, H. Yoshitome and H. Inoue, *J. Chem. Eng. Jpn*, 1983, **16**, 120.
- 9 V. Havredaki and J. H. Petropoulos, *J. Membrane Sci.*, 1983, **12**, 303.
- 10 C. Savvakis, K. Tsimillis and J. H. Petropoulos, *J. Chem. Soc., Faraday Trans. 1*, 1982, **78**, 3121.
- 11 T. L. Hill, *J. Chem. Phys.*, 1956, **25**, 730.
- 12 D. Nicholson and J. H. Petropoulos, *J. Phys. D*, 1968, **1**, 1379.
- 13 W. A. Steele in *The Solid-Gas Interface*, ed. E. A. Flood (Marcel Dekker, New York, 1967), vol. 1, chap. 10.
- 14 D. H. Everett and J. C. Powl, *J. Chem. Soc., Faraday Trans. 1*, 1976, **72**, 61.
- 15 W. A. Steele and G. D. Halsey Jr, *J. Phys. Chem.*, 1955, **59**, 57.
- 16 W. A. Steele, *Interaction of Gases with Solid Surfaces* (Pergamon Press, Oxford, 1974), chap. 2 and 3.
- 17 J. H. Petropoulos, *J. Membr. Sci.*, in press.
- 18 e.g. F. Ricca, C. Pisani and E. Garrone, *J. Chem. Phys.*, 1969, **51**, 4079.
- 19 e.g. C. Savvakis and J. H. Petropoulos, *J. Phys. Chem.*, 1982, **86**, 5128.
- 20 J. H. Petropoulos, *J. Chem. Soc., Faraday Trans. 1*, in press.
- 21 R. M. Barrer and J. H. Petropoulos, *Surf. Sci.*, 1965, **3**, 126.